ELSEVIER

Polymer 40 (1999) 3275–3289

polymer

Porous poly(L-lactide) films obtained by immersion precipitation process: morphology, phase separation and culture of VERO cells

R.A. Zoppi[a,*], S. Contant[a], E.A.R. Duek[b], F.R. Marques[c], M.L.F. Wada[c], S.P. Nunes[d]

[a]*Instituto de Química, Universidade Estadual de Campinas, C.P. 6154, CEP 13083-970, Campinas SP, Brazil*
[b]*Faculdade de Engenharia Mecânica, Universidade Estadual de Campinas, 6122, CEP 13083-970, Campinas SP, Brazil*
[c]*Instituto de Biologia, Universidade Estadual de Campinas, CEP, 13083-970, Campinas SP, Brazil*
[d]*GKSS-Forschungszentrum, 21502 Gessthacht, Germany*

Received 16 March 1998; received in revised form 18 June 1998; accepted 14 July 1998

Abstract

In this work, the immersion precipitation process was used to obtain porous poly(L-lactide) films which were tested as supports for culture of VERO cells. The mechanism of phase separation taking place during the film formation was investigated using light scattering measurements. A theoretical ternary phase diagram was proposed and correlated with the light scattering results. The film morphology was investigated using scanning electron microscopy. For films with a more porous surface, VERO cells grew with a round shape. For films with a lower surface porosity, the growth of flatter cells was observed. These preliminary tests show that the film morphology can affect the growth of cells, or can further change the cells' functions.

Keywords: Poly(L-lactide); Film morphology; Phase separation

1. Introduction

The growing interest in materials for applications in the human body led to a new area of research, concerned with the development of biomaterials, materials which assume the functions of tissue in natural organs or organ parts. They must therefore imitate the properties of such tissues as well as possible. A wide variety of polymeric biomaterials are currently being used in applications such as plastic and reconstructive surgery, dentistry, bone, muscle repair and support for cell culture. The latter is an interesting application, since isolated cells cannot form new tissues on their own, requiring a specific environment that very often includes the presence of a support material which can act both as a physical support and an adhesive substrate for isolated cells during the in vitro culture and subsequent implantation. A three-dimensional, porous and mechanically stable structure is desirable for cell growth, as it may occur in natural regeneration, for instance reconstruction of bone and cartilage. A uniformly distributed and interconnected pore structure should be formed to make possible the cell distribution throughout the device and an organized network of tissue constituents.

Polylactides, particularly poly(L-lactide), are organic polymers used frequently in the preparation of porous supports, due mainly to their very good biocompatibility. A general procedure that is used for obtaining poly(L-lactide) porous supports includes the preparation of a polymer solution which contains sodium salts (normally NaCl) with a controlled particle size. After solvent evaporation, films containing well distributed salt particles are obtained. The subsequent extraction of the salt, for example after washing with water, produces porous films in the range of 100–500 μm [1,2]. A different method has been reported by Mooney et al., who described the preparation of highly porous sponges using high pressure carbon dioxide processing at room temperature, which avoids the use of organic solvents and provides a simple and inexpensive method for producing useful devices in cell culture [3]. Other procedures which have been used to obtain porous supports include the gel-casting [4,5] and emulsion freeze-drying methods [6].

Phase separation techniques have become an important procedure to obtain porous structures, especially in the field of polymer membranes. Phase separation of polymer solutions can be induced in several ways, for instance thermally induced phase separation, air-casting of the polymer solution, precipitation from the vapor phase and immersion precipitation. In the latter case, the polymer solution is

* Corresponding author. Tel.: + 55-19-788-3039; Fax: + 55-19-788-3023 or + 55-19-239-3805; E-mail: rita@iqm.unicamp.br

0032-3861/99/$ - see front matter
PII: S0032-3861(98)00562-X

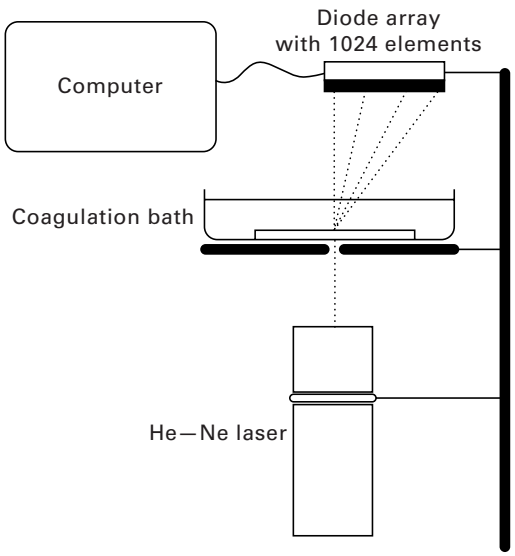

Fig. 1. Experimental system for light scattering measurements.

cast as a thin film, for example on a glass plate, which is subsequently immersed in a non-solvent bath. Phase separation and gelation in solution are responsible for the pore generation and for the fixation of the porous morphology.

Some works covering experimental and theoretical research related to the formation of polylactide films by immersion precipitation have been published [7–13]. Phase separation and morphology of the films prepared from polylactide–chloroform–methanol, polylactide–dioxane–methanol/water and polylactide–*N*-methylpyrrolidone–water systems have been emphasized, with determination of cloud points, osmotic pressure and other physical chemical properties.

In this paper, an immersion precipitation process was used to obtain porous poly(L-lactide) films which were tested as supports for culture of VERO cells. The mechanism of phase separation occurring during film formation was investigated by light scattering measurements. A theoretical ternary phase diagram was proposed and correlated with the light scattering results. The film morphology was investigated using scanning electron microscopy.

2. Experimental

2.1. Materials

Poly(L-lactide) (PLLA) was purchased from Medisorb-Du Pont ($Mw = 300\ 000\ g\ mol^{-1}$). Chloroform and ethanol were obtained from Nuclear and were of analytical quality.

2.2. Film preparation

Films were prepared by casting the chloroform–PLLA solution on a glass plate, normally used as sample holders for optical microscopy, and immediately introduced into the coagulation bath. The temperature of the bath was kept at $25 \pm 2°C$. The initial casting thickness was 200 μm. Coagulation baths with the following ethanol–chloroform (wt%) compositions were used: 100:0, 90:10, 80:20, 70:30, 60:40 and 50:50. Ethanol–chloroform solutions were prepared by mixing different amounts of ethanol and chloroform in order to obtain the final desired composition. The mixture was stirred for 10 min at room temperature before use. The solvents were used as received.

2.3. Light scattering measurements

The system for light scattering measurements has been described previously [14]. It consists of a He–Ne laser ($\lambda = 633$ nm), which was used as a light source (Fig. 1). A diode array produced by Cronic Electronic, with a total length of 26 mm, containing 1024 elements, separated from each other by 25 μm, was used as detector, orthogonal to the laser beam and connected to a computer by an interface card.

The total range of angles covered by the detector could be adjusted by moving the diode array in relation to the sample. For the experiments described here, the diode array was positioned at 2.5 cm above the sample, allowing simultaneous measurements of the light scattering by the sample at angles from 0 to ca. 40° (covered by a total of 1024 points). The software permitted the acquisition of a series of 24 integrated measurements (with 1024 points each), separated by time intervals varying from 1 to 20 s. The period, during which the signal for each measurement was accumulated (integrated), could also be adjusted and a period from 10 to 35 ms was typically chosen, being long enough to allow a good detection of the scattered light. In the choice of this parameter, it was also taken into account that the period should be short enough to avoid detector saturation. For the same reason, the experiment was performed in a dark room. The acquisition period was also short enough to discard any contribution due to disturbances in the coagulation bath. Measurements without the polymer film were performed previously to confirm that no disturbance would affect the scattered light detection.

For the measurements, a Petri dish was located between the laser and the diode array containing the coagulation bath (ethanol–chloroform mixtures). A thin layer of polymer solution was cast on a glass plate, as described above, and immediately introduced into the coagulation bath. The detection was started simultaneously, by pressing a key of the computer keyboard, and 24 consecutive measurements were recorded automatically.

2.4. Scanning electron microscopy

The films prepared as described above were dried under a vacuum during one day. They were fractured in liquid nitrogen and the cross-sections were coated with gold by sputtering. The fracture surface was observed in a JEOL JXA-840 scanning electron microscope.

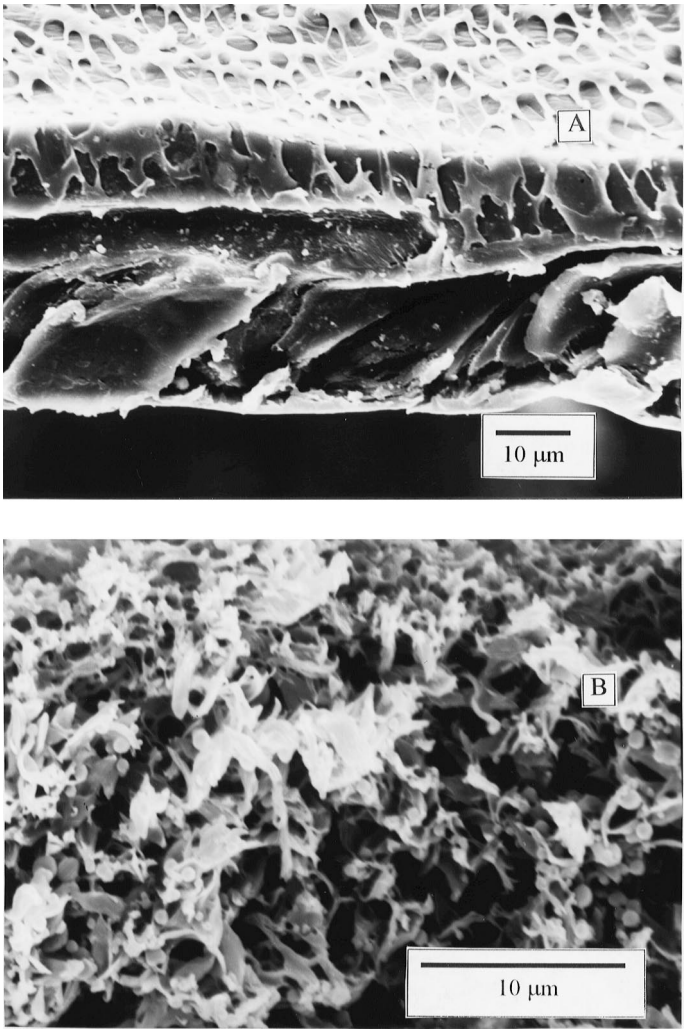

Fig. 2. Scanning electron micrographs (cross-section) of: (A) a film prepared from 98:2 (weight) $CHCl_3$–PLLA solution by immersion in water and (B) a film prepared from 88:10:2 (weight) $CHCl_3$/*N*,*N*-dimethylformamide–PLLA solution by immersion in ethanol.

2.5. Cell culture experiments

The porous films were washed in a 0.9% saline solution, autoclaved for 30 min at 121°C and immersed in Ham F10 medium with 10% fetal calf serum for 24 h at 37°C. VERO cells (7×10^6 cells ml^{-1}) were inoculated in Leighton tubes containing a glass coverslip half covered with a porous polymer film.

After 120 h of incubation, the polymer film and coverslips were fixed following the procedure described by Karnovsky [15], washed in water, dehydrated in a graded series of ethanol–water solutions, cleared in xylol and paraffin embedded.

Thin sections (7 μm) were stained with Toluidine Blue and Cresol Violet at pH 4.0 [16], and the coverslips were mounted with Entelan (Merck).

Scanning electron microscopy was carried out following the procedure described by Grinnell and Bennett [17]. The coverslip and polymer films were first fixed in glutaraldehyde (3%) for 4 h at 4°C, followed by fixation in a 1% OsO_4 solution for 1 h at 4°C, dehydrated in a graded series of ethanol–water solutions, dried at the critical point and finally sputtered with a layer of gold.

3. Results and discussion

3.1. Morphology of the porous films: effect of polymer concentration, composition of immersion bath and presence of additives

Figs. 2 and 3 show scanning electron micrographs of porous films prepared from dilute PLLA solutions (98:2 or 96:4 (by weight) $CHCl_3$–PLLA) by immersion in water, ethanol or ethanol–$CHCl_3$ mixtures. Using water as non-solvent, dense films were obtained with an apparently porous skin. Similar structures were reported in the literature [11] for polylactide–dioxane–water systems. On the other hand, using ethanol as non-solvent, a uniform porous structure with cellular morphology was obtained (Fig. 3A).

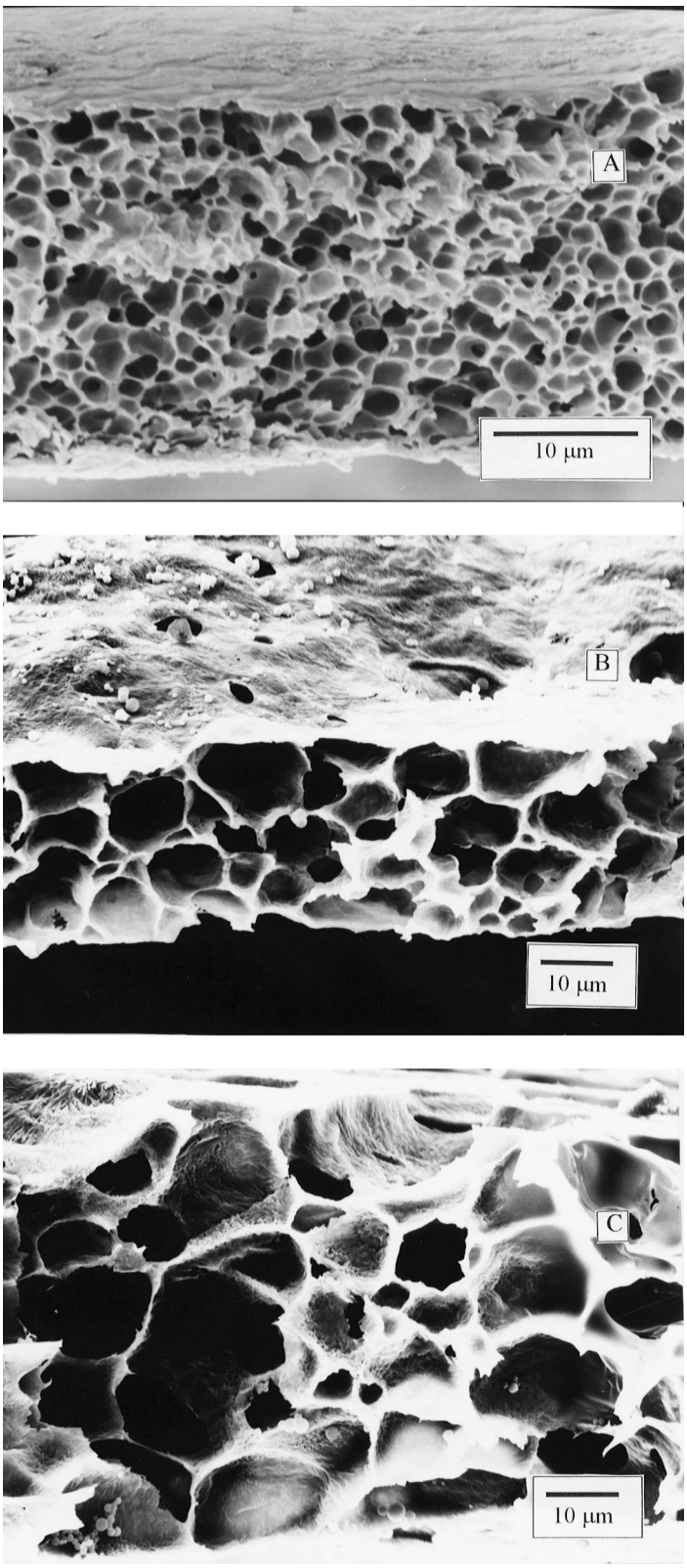

Fig. 3. Scanning electron micrographs (cross-section) of films prepared from 96:4 (weight) $CHCl_3$–PLLA solutions by immersion in (by weight) 100:0 (A), 70:30 (B) and 60:40 (C) ethanol–$CHCl_3$ baths.

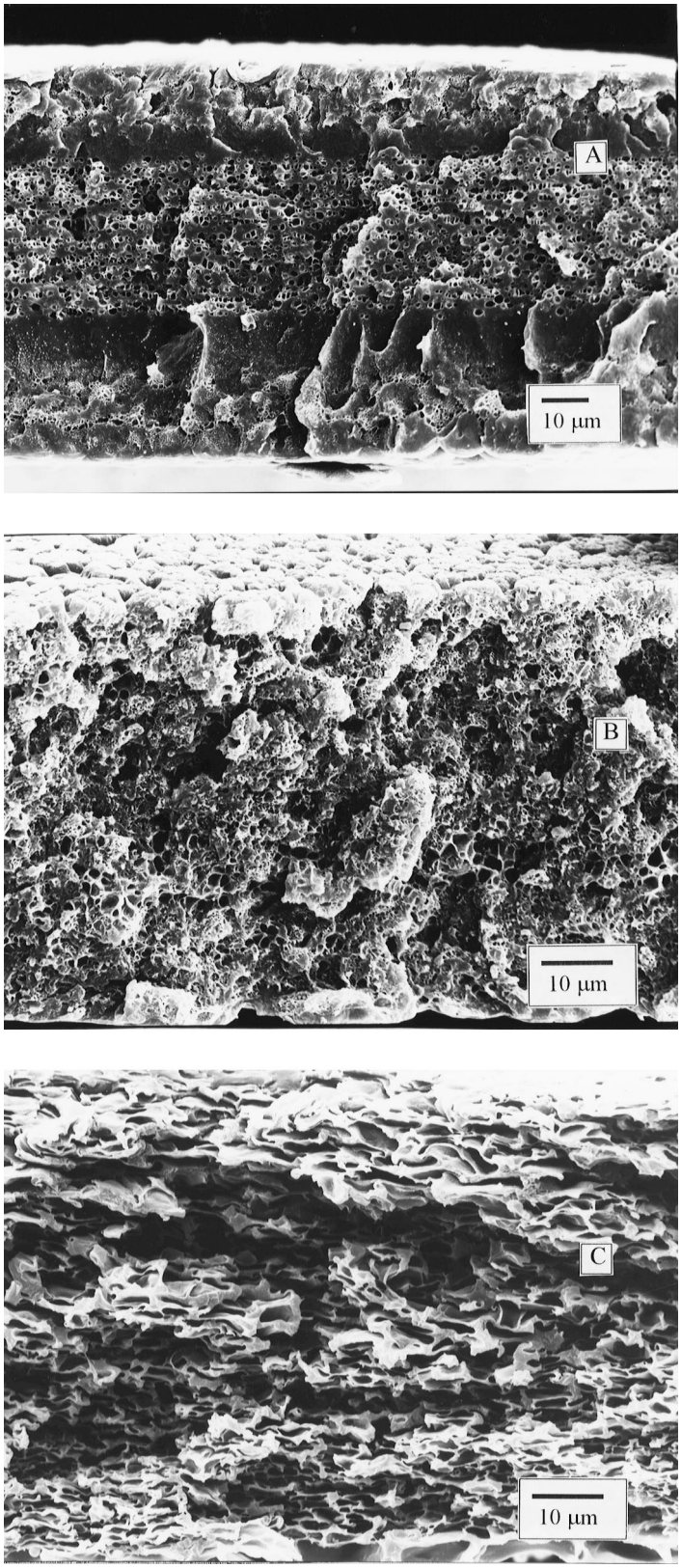

Fig. 4. Scanning electron micrographs (cross-section) of films prepared from (by weight) 80:20 $CHCl_3$–PLLA solutions by immersion in (by weight) 100:0 (A), 90:10 (B) and 60:40 (C) ethanol–$CHCl_3$.

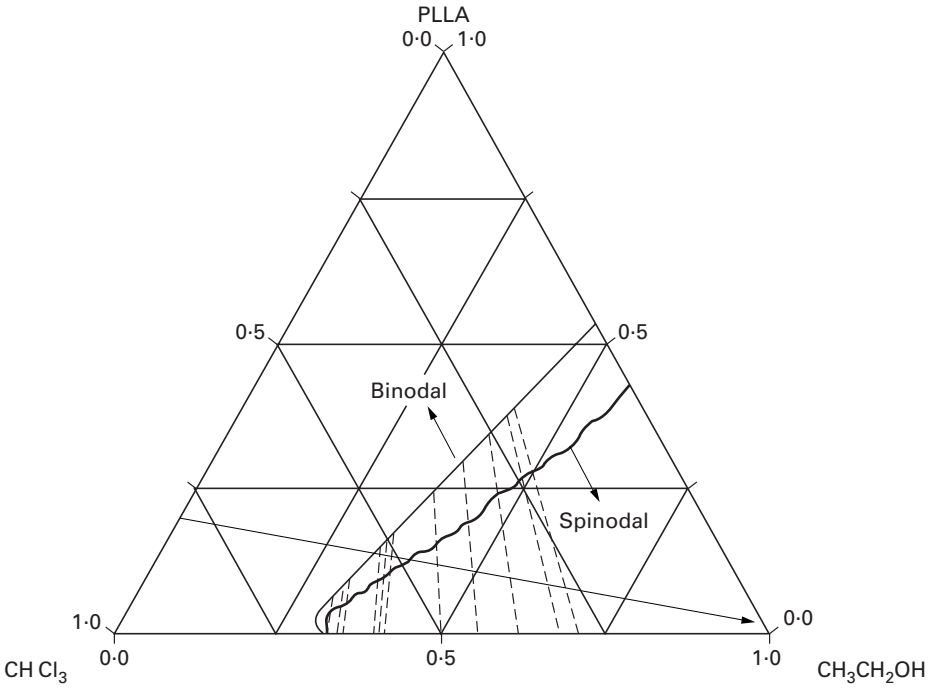

Fig. 5. Phase diagram calculated for the PLLA–chloroform–ethanol system. Interaction parameters used for calculation were $\chi_{PLLA-chloroform} = 0.4$, $\chi_{PLLA-ethanol} = 1.0$ and $\chi_{chloroform-ethanol} = 0.3$.

As the immersion bath composition changed with increasing content of $CHCl_3$, similar cellular structures were still observed, but with increasing cell size, varying from 5 μm (minor porous in Fig. 3B) to more than 10 μm (larger porous in Fig. 3C).

Films prepared from more concentrated casting solutions had a much different, denser morphology (Fig. 4). As the $CHCl_3$ content in the immersion bath increased to 40 wt%, a cellular morphology (with small cells) was again observed. The formation of porous cellular structures has often been assigned to liquid–liquid demixing [14]. However, for crystallizable polymers such as PLLA, solid–liquid demixing can play an important role in structure formation. Both liquid–liquid and solid–liquid demixing are probably competing in the formation of PLLA films. These morphological differences can be better understood by considering the phase diagram of the PLLA–chloroform–ethanol system, discussed below.

The composition of the casting solution was also changed by adding *N*,*N*-dimethylformamide (DMF) in an attempt to enlarge the pores. However, when the PLLA content was higher than 2 wt%, practically no change was observed. For even more diluted polymer solutions, a drastic influence on the film morphology was observed due to the presence of DMF: the cellular morphology was completely deformed (Fig. 2B).

3.2. Phase diagram

To better understand the light scattering results, the phase diagram of the PLLA–$CHCl_3$–ethanol system will first be considered. Fig. 5 shows the ternary phase diagram calculated for the system from the data of interaction parameters, $\chi_{PLLA-chloroform} = 0.4$, $\chi_{PLLA-ethanol} = 1.0$ and $\chi_{chloroform-ethanol} = 0.3$, using a calculation method based on the Gibbs energy of mixing, but which does not require the derivatives of the Gibbs energy [18,19]. The polymer–solvent and polymer–non-solvent interaction parameters were extracted from the literature [12], and the solvent–non-solvent parameter was calculated considering the chloroform and ethanol solubility parameters.

In a ternary phase diagram, the corners represent the pure components and the axes the three binary combinations. The phase diagram is divided into a homogeneous region and an area representing a liquid–liquid demixing gap. These regions are separated by the binodal curve. A metastable area exists between the spinodal and the binodal. The spinodal curve separates the unstable and the metastable regions. The dotted lines on the phase diagram are the tie lines, connecting the composition of the separated phases in the film at different quench depths. A system analogous to that described here consists of a solution whose initial composition could be represented on the PLLA–chloroform axis. During the solvent–non-solvent exchange, the solution composition changes progressively, crossing the phase diagram in the direction of the PLLA–ethanol axis. The final composition in the film is given by the total weight of polymer forming the film matrix and the total weight of ethanol to fill the pores. Almost all the solvent goes into the immersion bath. This composition path may be quite

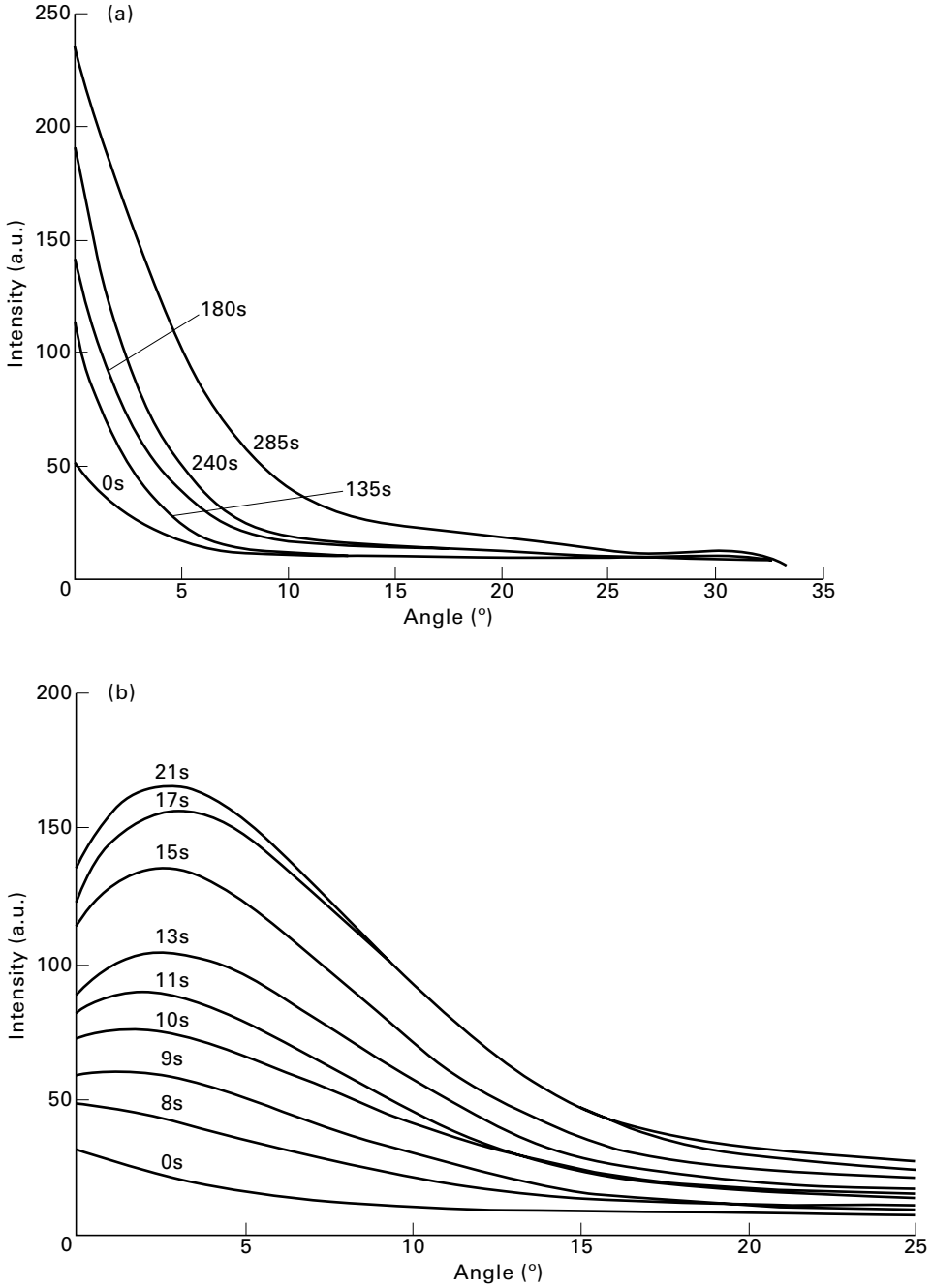

Fig. 6. Scattering patterns recorded during the preparation of films by immersion of 80:20 (a) or 96:4 (b) $CHCl_3$–PLLA solutions in ethanol.

complex [20,21] and it would be an oversimplification to assume that it would be a straight line connecting the starting and the final film compositions.

Nucleation and growth (NG) is the expected mechanism when a system leaves the thermodynamically stable condition and slowly enters the metastable region of the phase diagram, between the binodal and the spinodal curves. Dispersed nuclei are formed and become stable if the activation energy for nuclei formation is higher than their surface free energy. NG is usually a slow process and leads to a matrix/disperse domains morphology. Spinodal decomposition (SD) takes place in a fast quench into the two-phase region limited by the spinodal curve or even in a slower quench crossing the metastable region near the critical point. In this case, phase separation is initiated with concentration fluctuations of increasing amplitude, giving rise to two continuous phases, with a characteristic periodic interphase distance. If the process is 'frozen' early enough by a mobility change, a morphology with high interconnectivity is obtained. However, in the later stages of phase separation, coalescence may also take place, leading to a matrix/disperse domains morphology. SD is normally much

Table 1
Mechanisms of phase separation for $CHCl_3$–PLLA casting solutions in immersion baths with different ethanol–$CHCl_3$ contents: apparent diffusion coefficient, D_{app} ($\mu m^2\ s^{-1}$), time to start demixing, t_D (s), and time to start gelation, t_G (s)

$CHCl_3$–PLLA solution	Ethanol–chloroform immersion baths					
	100:0	90:10	80:20	70:30	60:40	50:50
98:2	SD $D_{app} = 0.90$ $t_D = 3$ $t_G = 6$	SD $D_{app} = 0.93$ $t_D = 3$ $t_G = 6$	SD $D_{app} = 0.10$ $t_D = 72$ $t_G = 90$	SD $D_{app} = 0.11$ $t_D = 36$ $t_G = 54$	NG $K = 6e - 10$ $n = 4, 5$ $t_D = 182$	1 phase
96:4	SD $D_{app} = 0.37$ $t_D = 11$ $t_G = 16$	SD $D_{app} = 0.26$ $t_D = 12$ $t_G = 21$	SD $D_{app} = 0.14$ $t_D = 27$ $t_G = 36$	SD $D_{app} = 0.07$ $t_D = 56$ $t_G = 68$	NG $K = 6e - 17$ $n = 7, 2$ $t_D = 272$	1 phase
92:8	SD $D_{app} = 0.20$ $t_D = 6$ $t_G = 10$	NG $K = 6e - 5$ $n = 3, 6$ $t_D = 32$	NG $K = 1e - 5$ $n = 4, 5$ $t_D = 24$	NG $K = 6e - 6$ $n = 3, 8$ $t_D = 52$	NG $K = 1e - 6$ $n = 3, 2$ $t_D = 180$	1 phase
90:10	SD $D_{app} = 0.25$ $t_D = 16$ $t_G = 20$	NG $K = 6e - 3$ $n = 3, 1$ $t_D = 16$	NG $K = 1e - 6$ $n = 4, 3$ $t_D = 44$	NG $K = 5e - 6$ $n = 3, 6$ $t_D = 66$	NG $K = 4e - 9$ $n = 4, 1$ $t_D = 225$	1 phase
85:15	SD $D_{app} = 0.10$ $t_D = 80$	NG $K = 6e - 7$ $n = 4, 2$ $t_D = 64$	NG $K = 3e - 5$ $n = 3, 3$ $t_D = 70$	NG $K = 6e - 4$ $n = 2, 1$ $t_D = 150$	NG $K = 7e - 5$ $n = 2, 4$ $t_D = 180$	1 phase
80:20	NG $K = 6e - 3$ $n = 1, 8$ $t_D = 135$	NG $K = 4e - 2$ $n = 2, 4$ $t_D = 131$	NG $K = 6e - 2$ $n = 2, 5$ $t_D = 130$	NG $K = 3e - 6$ $n = 5, 6$ $t_D = 137$	NG $K = 2e - 5$ $n = 2, 6$ $t_D = 160$	1 phase

faster than NG. Considering only the phase diagram of the PLLA–chloroform–ethanol system, since the critical point is very near the chloroform–ethanol axis, more dilute PLLA casting solutions have a higher probability to demix by SD than more concentrated solutions.

3.3. Light scattering measurements

Light scattering measurements have been used previously for the investigation of phase separation mechanisms. A detailed description of the light scattering theory for phase separation is given in Ref. [14].

It is important to mention here that the phase separation detected by light scattering corresponds to the formation of the film skin immediately in contact with the immersion bath. Demixing does not take place simultaneously in the whole film. It starts at the skin and continues progressively. Different layers may reach the thermodynamic condition for demixing, entering the two-phase region of the phase diagram at different points. Therefore, one cannot neglect the idea that different mechanisms of phase separation may take place in different layers of the same film, but only demixing of the layer directly in contact with the immersion bath can be observed by light scattering.

In this work, the following $CHCl_3$–PLLA casting solutions with polymer content varying from 2 to 20 wt% were investigated. A thin film of each solution was immersed in coagulation baths with the following ethanol–$CHCl_3$ (wt%) compositions: 100:0, 90:10, 80:20, 70:30, 60:40 and 50:50. All the solutions immersed in the 50:50 ethanol–$CHCl_3$ bath did not demix.

The phase separation was detected by light scattering measurements using the diode array. Analyzing the angle dependence of the light scattered in different conditions, either a monotonic intensity decrease or halo scattering patterns were recorded, as shown in Fig. 6. The former behavior was connected to the NG mechanism and the latter to the SD mechanism. Table 1 summarizes the mechanisms of phase separation detected by light scattering for polymeric solutions of different concentrations in different immersion baths. NG is predominant in immersion baths with lower ethanol content and therefore near the condition

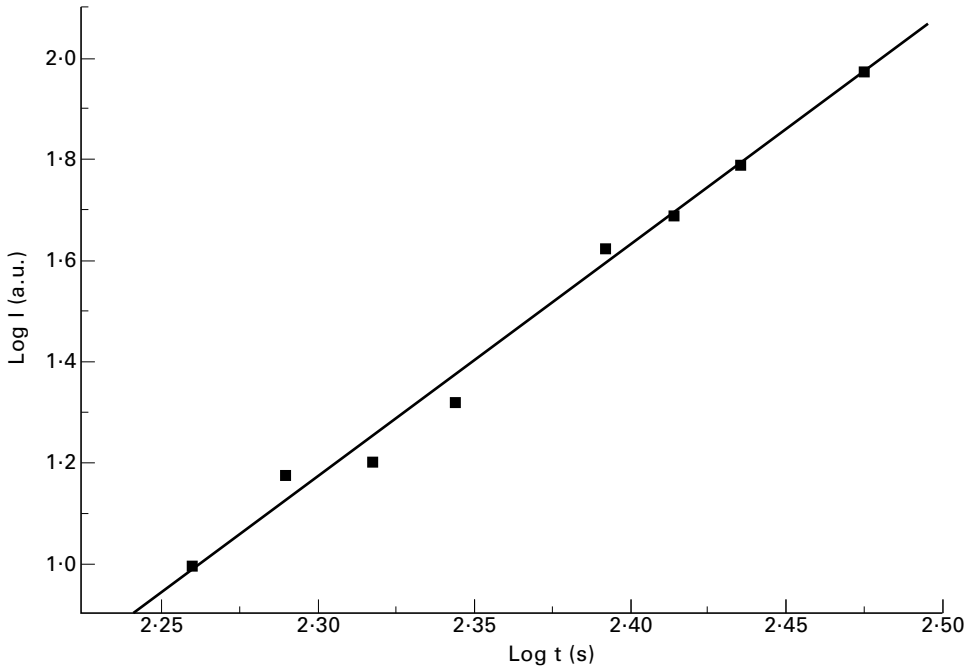

Fig. 7. Log I vs. log t for films prepared from 98:2 $CHCl_3$–PLLA solutions by immersion in a 60:40 ethanol–chloroform bath.

for which no phase separation is expected. NG also prevails for casting solutions with higher polymer concentrations. The critical point for PLLA–$CHCl_3$–ethanol, where spinodal and binodal curves touch, is located at very low polymer concentrations, as can be seen in the phase diagram. When working with diluted casting solutions, the metastable region can be easily and rapidly crossed by solvent exchange, reaching conditions which favor SD. When more concentrated casting solutions are immersed in the coagulation bath, the system remains for a long time in the metastable region, which is wider in the middle of the phase diagram, and NG is again favored.

When the NG mechanism predominates, at a fixed angle, the increase of scattering light intensity can be fitted according to a power law [22]:

$$I = K(t - \tau)^n, \tag{1}$$

where I is the scattered light intensity at a fixed angle, K is the growth constant, t is the time and τ is the time when nucleation starts (usually taken as equal zero). If results can be well fitted in a log I vs. log $(t - \tau)$ plot, giving a straight line with a slope close to 3 ($n = 3$), a heterogeneous nucleation mechanism is indicated. If the best fit is obtained with $n = 4$, homogeneous nucleation is suggested.

Characteristic curves of a phase separation by nucleation and growth were analyzed according to Eq. (1). A typical curve of log I vs. log t is shown in Fig. 7 for films prepared from 98:2 $CHCl_3$–PLLA solution by immersion in a 60:40 ethanol–chloroform bath. In this particular case, the n value was 4.5, which is close to that expected for homogeneous nucleation. However, for several films the best fit gives n values which are very different from 3 or 4, as shown in Table 1, and no conclusion should be drawn concerning the kind of nucleation (heterogeneous or homogeneous). Table 1 shows also the values for the growth constant K and time to start demixing from the moment the solution has been immersed. As a general tendency, higher K values were obtained for solutions immersed in baths with higher ethanol content. Demixing also starts earlier in baths with higher ethanol content. This is expected, since ethanol is the non-solvent and in baths with higher ethanol content the thermodynamic condition for phase separation is reached after just a short solvent–non-solvent exchange.

For the SD investigation, results are normally treated by the linear Cahn–Hilliard theory [23]. According to this theory, light passing through a system with phase separation taking place by spinodal decomposition is diffracted, forming a scattering halo. During spinodal decomposition, each concentration fluctuation with a wavenumber q contributes to diffraction at an angle θ:

$$q = (4\pi/\lambda)\sin(\theta/2), \tag{2}$$

where λ is the wavelength of the incident light.

Some fluctuations with a wavelength q_m are predominant and contribute to a maximum scattered light intensity at an angle θ_m, giving rise to the observed halo. In the early stages of SD, q_m does not vary, only the amplitude of each concentration fluctuation is increased, and the scattered light intensity at a fixed angle increases exponentially with time. To confirm that phase separation is taking place by spinodal decomposition, other arguments also have to be fulfilled. According to the Cahn–Hilliard linear theory, the slope of a log I vs. t plot at a fixed angle θ gives $R(q)$, the amplitude

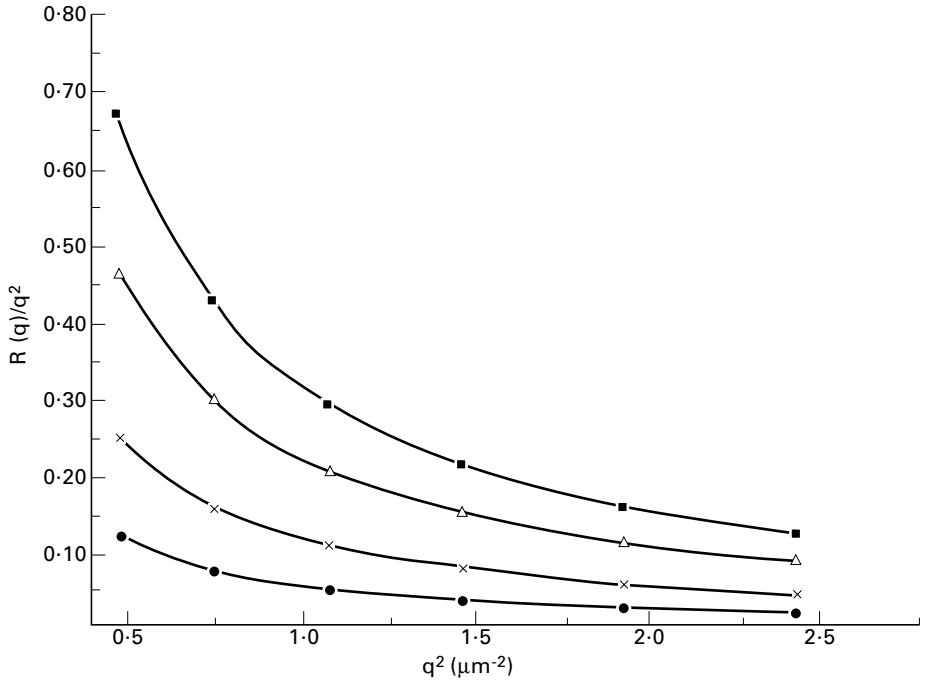

Fig. 8. $R(q)/q^2$ of films prepared from the 96:4 $CHCl_3$–PLLA solution by immersion in ethanol–chloroform baths of different compositions. (■) 100:0; (△) 90:10; (×) 80:20; (●) 70:30.

growth rate of fluctuations with wavenumber q:

$$I(q,t) \cong \exp[2R(q)t]. \quad (3)$$

In systems with spinodal decomposition, following the Cahn–Hilliard theory, plots of $R(q)/q^2$ vs. q^2 are linear, and the extrapolation to $q = 0$ allows the estimation of the apparent diffusion coefficient, D_{app}, which expresses how fast the phase separation takes place.

For the PLLA–chloroform–non-solvent systems investigated here, those cases with a scattering halo were analyzed according to the Cahn–Hilliard theory. Typical $R(q)/q^2$ vs. q^2 curves are shown in Fig. 8 for films prepared from 96:4 $CHCl_3$–PLLA solutions by immersion in ethanol–chloroform baths of different compositions. Similar patterns were also observed for other solutions with a scattering halo. A clear deviation from linearity is observed here, especially at lower q values. This may be due to instability caused during immersion of the film in the bath or temperature fluctuations due to the solvent and non-solvent exchange, but another possibility cannot be disregarded: the phase separation in this system may not follow a linear theory. $R(q)/^2$ vs. q^2 tests the validity of the linear theory. In several systems [24], these curves are, however, non-linear. In these cases, a non-linear theory, such as that proposed by Langer et al., may be more convenient, incorporating nonlinear effects (particularly, higher order terms related to the composition fluctuations) on the diffusion equations for spinodal decomposition [25]. Cook [26] had also modified the Cahn–Hilliard theory, introducing a term which represents thermal fluctuations in the linear diffusion equation. The data presented here should therefore be treated with a more complex theory to be fully described. However, to obtain relative information on how fast the process of phase separation is, D_{app} values were calculated neglecting the points at low q, and are presented in Table 1. It can be clearly seen that the phase separation is much faster when the PLLA solution is immersed in ethanol and is progressively slower as the immersion bath becomes richer in chloroform, since the thermodynamic condition for the polymer is much worse in baths with higher ethanol content. In other words, immersion of casting solutions in baths with higher ethanol content leads to deeper quenching into the unstable region of the phase diagram. The apparent diffusion coefficient, D_{app}, is lower when phase separation occurs at conditions near the spinodal curve. Also, as the polymer concentration in the casting solution is increased, D_{app} decreases, since the viscosity of concentrated solutions is higher and the chain mobility is lower, therefore leading to slow demixing. For the same reasons, the time necessary to start phase separation is longer for more concentrated solutions.

The time to start gelation was estimated here assuming that the deviation from linearity of the log I vs. t curves is caused by a change in the system viscosity. Higher gelation times were observed in immersion baths with lower ethanol contents.

3.4. Phase separation behavior and final morphology of the films

The results shown in Table 1, in addition to the calculated

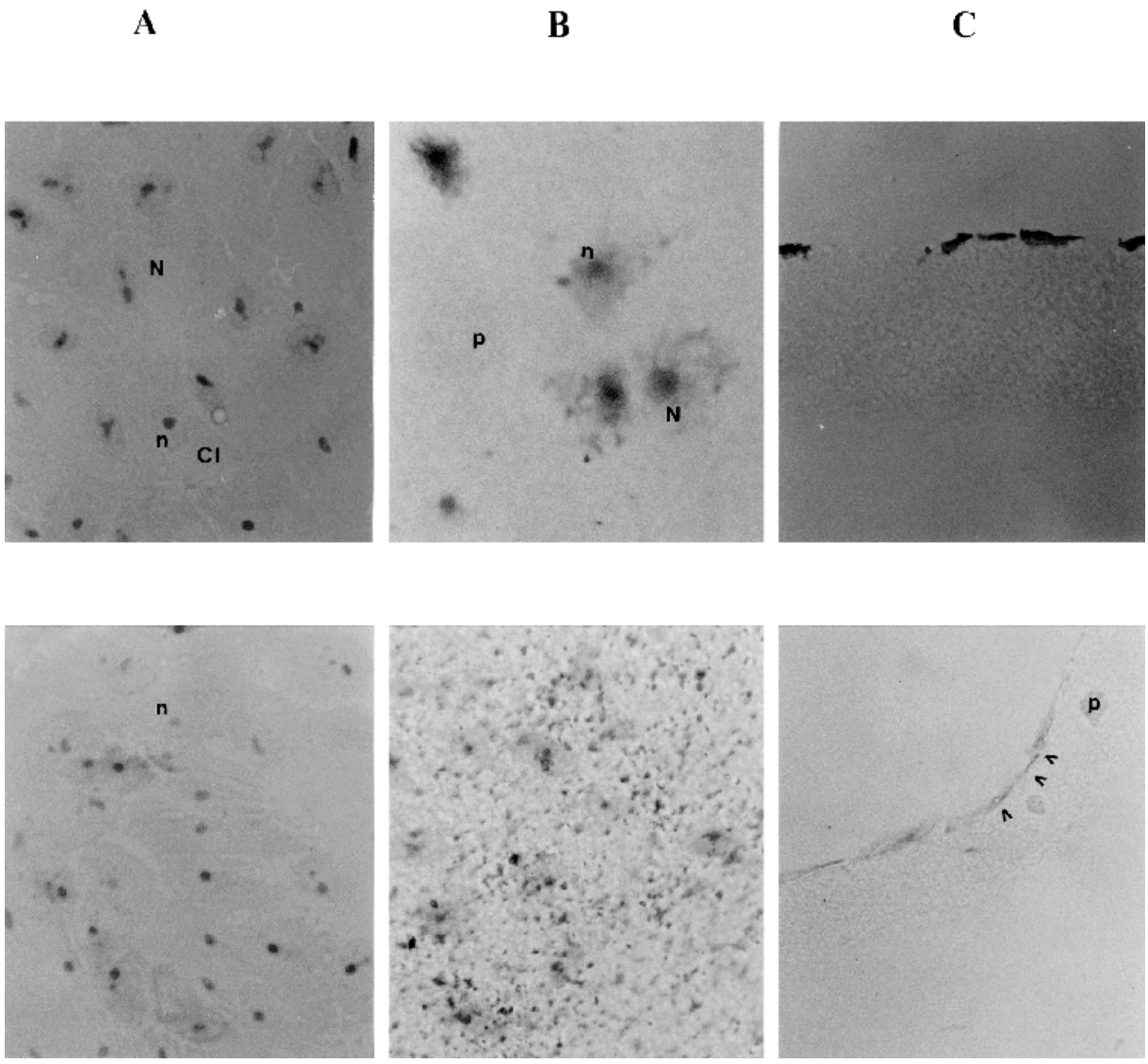

Fig. 9. Optical microscopy of VERO cells grown for 72 h in Leighton tubes on glass coverslips (A) and porous polymer films (B; area 1 cm^2). Top: polymer films prepared from 88:10:2 $CHCl_3$–*N*,*N*-dimethylformamide–PLLA solutions. Bottom: polymer films prepared from 96:4 $CHCl_3$–PLLA solutions. (C) Cross-sections of the porous polymer films stained with Toluidine Blue. ∧ ∧ ∧, basal membrane; N, nuclei; n, nucleolus; p, polymer; CI, cytoplasm.

phase diagram, can be used to better understand the final morphologies observed for PLLA films.

By observing the calculated phase diagram and assuming that the path for phase separation occurring can be described by the arrow which leaves the PLLA–chloroform axis, it can be noted that, for more concentrated $CHCl_3$–PLLA solutions, phase separation could take place by the NG mechanism. For more dilute $CHCl_3$–PLLA solutions, the heterogeneous region of the phase diagram would be entered almost directly, i.e. practically without passing through the metastable region. In these cases, the phase separation could occur by the SD mechanism. These observations agree with the results shown in Table 1, for an ethanol–chloroform bath with composition 100:0.

The porous cellular-type morphology has been assigned to the liquid–liquid phase separation that occurs by nucleation and growth of a poor polymer phase, with the fixation and stabilization of the cellular structure occurring by crystallization, in the case of crystalline polymers.

For more dilute $CHCl_3$–PLLA solutions, independently of the ethanol–chloroform bath composition, a porous cellular morphology was observed, even for systems demixing by spinodal decomposition. This behavior could be associated with the coalescence phenomenon which can take place in systems demixing by spinodal decomposition, leading to a matrix/disperse domain morphology. Then, a morphological analysis alone may be inconclusive regarding the investigation of phase separation mechanisms.

With respect to films prepared from 80:20 $CHCl_3$–PLLA solutions, the observed morphology may be a result of a gradual inversion of the phase separation sequence, with the crystallization process taking place before liquid–liquid

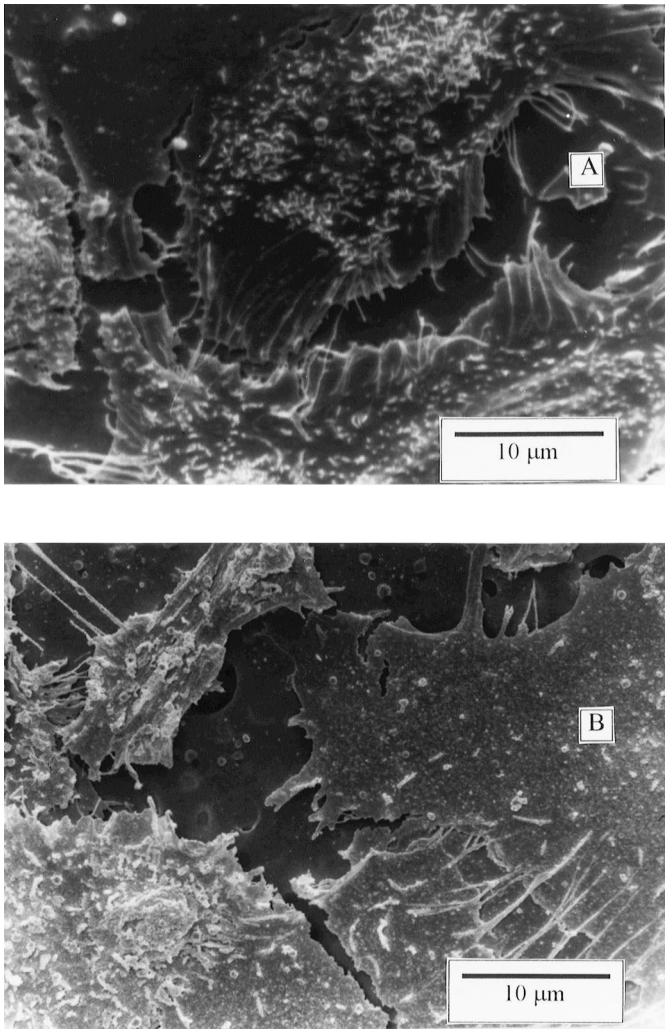

Fig. 10. Scanning electron microscopy of VERO cells grown by 120 h into Leighton tubes on (A) glass coverslips and polymer films (area 1 cm^2) prepared from (B, D) 96/4 $CHCl_3$PLLA solutions and from (C) 88/10/2 $CHCl_3$/*n*, *n*-dimethylformamide/PLLA solutions. (D) Detail of the film surface before the cell growth.

demixing. In these cases, isolated spherulites or spherulites surrounded by a porous cellular layer would be observed, as reported by van de Witte and co-workers [12].

It is important to bear in mind that the transitions that occur during the preparation of porous films by phase inversion are due to the porous structure generation and the morphology fixation. During demixing, the rich polymer phase is fixed by an abrupt decrease of the polymer chain mobility, which can have different causes, such as crystallization or vitrification, as well as changes in the polymer–solvent interaction.

Witte and co-workers have investigated the phase behavior of semi-crystalline PLLA and amorphous poly(DL-lactic acid) [12]. They determined solubility curves, cloud point curves and vitrification boundaries for some poly(lactic acid)–solvent–non-solvent systems. Considering the solubility curve at 25°C for the PLLA–chloroform–ethanol system [12], one can expect that the crystallization process could occur when $CHCl_3$–PLLA solutions with concentrations greater than 10 wt% are used for preparing porous films, since it would be possible to cross the solubility curve (pass through a liquid–solid transition) before liquid–liquid demixing occurs.

Changing the immersion bath composition (by adding chloroform to the ethanol bath), the polymer–non-solvent and solvent–non-solvent interaction parameters have a tendency to decrease. This variation promotes a decrease of the heterogeneous region of the phase diagram. In addition, the solubility curve and vitrification boundary can be shifted. Then, even for films prepared from more concentrated solutions, a cellular-type morphology (typical of nucleation and growth demixing) could be obtained. This process seems to occur for films prepared from 80:20 $CHCl_3$–PPLA solutions by immersion into the 60:40 ethanol–chloroform bath. Its morphology is closer to that observed for films which were prepared from more dilute polymer solutions, i.e. liquid–liquid demixing probably took place before crystallization.

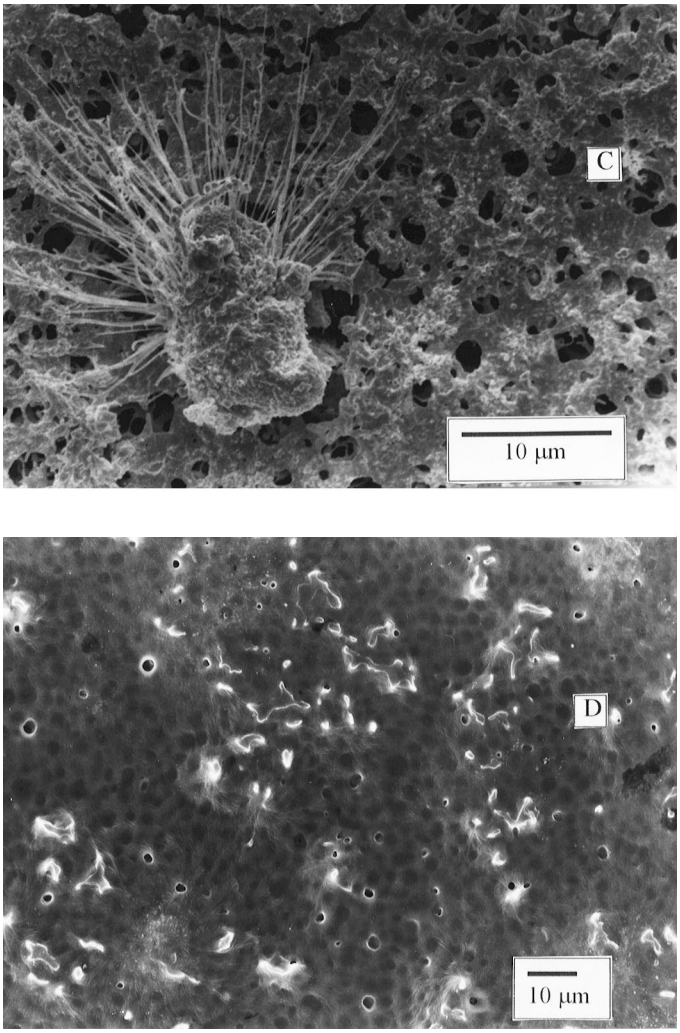

Fig. 10. Continued.

Using water as a non-solvent, the morphology of the films was very different from that observed for films prepared in a less polar non-solvent, e.g. ethanol. As shown in Fig. 2A, dense films containing only a porous skin on their surface were obtained. Apart from thermodynamic parameters, kinetic parameters will also play an important role in the phase separation process. Low solvent–non-solvent exchange rates will promote solid–liquid demixing processes that are favored thermodynamically. For the exchange rate, it has been demonstrated that a good solvent–non-solvent interaction, coupled to high mutual diffusion coefficients, will usually result in a very rapid exchange of solvent for non-solvent, promoting liquid–liquid demixing over solid–liquid demixing [8]. Chloroform–water is a solvent–non-solvent combination with low compatibility and mutual affinities (high $\chi_{\text{solvent–non-solvent}}$). The phase separation will take place more slowly. The solvent–non-solvent exchange rate is probably too slow to allow phase separation over the whole extension of the cast film, resulting in a heterogeneous morphology, as seen in Fig. 2A.

3.5. Culture of VERO cells

Cellular growth was tested in two types of porous polymer films: those prepared from 88:10:2 $CHCl_3$–*N*,*N*-dimethylformamide–PLLA solutions and those prepared from 96:4 $CHCl_3$–PLLA solutions (Fig. 9). In both cases, an ethanol bath was used for immersion. Cellular growth was independent of the procedure adopted for the film preparation, suggesting that the material under study is innocuous to the cells. VERO cells grown on the polymeric films were morphologically similar to fibroblast cells, with apparent nuclei and nucleolus, as seen in Fig. 9. The presence of round as well as elongated cells was observed for the film prepared from 88:10:2 $CHCl_3$–*N*,*N*-dimethylformamide–PLLA solution, although the total number of cells found in this case was much smaller than that relative to the films prepared from 96:4 $CHCl_3$–PLLA solutions.

Analysis of the cross-sections of the polymeric films stained with Toluidine Blue (Fig. 9C) showed that cell growth occurred in a monolayer, without penetration of the pores. In these samples, the deposition of a material

slightly stained with Toluidine Blue below the cellular layer, and believed to be a basal membrane, was observed. The development of a cellular structure and the production of basal membrane components in cell cultures has already been cited in the literature by Golombick and co-workers [27], who reported that ovarian tumor cells produce collagen type IV and laminina. VERO cells grown on glass coverslips and on collagen type I also produce a basal membrane, and the presence of collagen type IV was also observed [28].

Fig. 10 shows the scanning electron micrographs of cells grown on different substrates. A similar behavior was observed for cell growth on both the glass coverslips and the polymeric substrates containing 4 wt% PLLA. Flat cells, indicative of adhesion and substrate coverage, were observed. The cells also showed microvilli as well as several philopodios on their edges. For films with lower surface porosity, i.e. those with 4 wt% PLLA content, cells with extensions and/or philopodios that either covered or deviated from the pores were observed (Fig. 10B). The fact that some of them deviated from the pores could explain the small number as well as the round shape of cells found on the surface of films prepared from 88:10:2 $CHCl_3$–*N*,*N*-dimethylformamide–PLLA solutions, which are highly porous and therefore have less surface area available for cell adhesion.

It must also be mentioned that cells were grown in a 10% fetal calf serum rich in elements, such as fibronectin, that promote cellular adhesion and growth. Fibronectin is one of the glycoproteins which are responsible for cell adhesion on the substrate, since cells present proteins called integrins which act as fibronectin receptors.

4. Conclusions

Poly(L-lactic acid) films with different morphologies can be obtained using the immersion precipitation process. The morphology seems to be a result of a complex interplay between solid–liquid demixing and liquid–liquid demixing, in which the polymer concentration of the casting solution can determine the sequence of these events.

Light scattering measurements supplied experimental evidence for the mechanism of phase separation during formation of the porous films. Nucleation and growth predominated in more concentrated polymer solutions. Spinodal decomposition was observed for more diluted polymer casting solutions and when the immersion bath had a higher ethanol content. Phase separation was faster as the polymer concentration was lowered and as ethanol was richer in the immersion bath.

Tests with VERO cells were performed. For films with a more porous surface, VERO cells grew with a round shape. For films with a lower surface porosity, the growth of flatter cells was observed. These preliminary tests show that the film morphology can affect the growth of cells, or can even change the cells' functions further.

Acknowledgements

We thank FAPESP (Proc. 95/9506-4, 95/6942-0, 96/2761-1, 96/5445-3) and CNPq for financial support.

References

[1] Lam KH, Nieuwenhuis P, Molenaar I, Esselbrugge H, Feijen J, Dijkstra PJE, Schakeraad JM. Biodegradation of porous versus non porous poly(L-lactic acid) films. J Mater Sci: Mater Med 1994;5:181.
[2] Wald HL, Sarakinos G, Lyman MD, Mikos AG, Vacanti JP, Langer R. Cell seeding in porous transplantation devices. Biomaterials 1993;14:270.
[3] Mooney DJ, Baldwin DF, Suh PS, Vacanti JP, Langer R. Novel approach to fabricate porous sponges of poly(D,L-lactide-co-glycolic acid) without the use of organic solvents. Biomaterials 1996;17:1417.
[4] Coombes AGA, Heckman JD. Gel casting of resorbable polymers. 1. Processing and applications. Biomaterials 1992;13:217.
[5] Coombes AGA, Heckman JD. Gel casting of resorbable polymers. 2. In vitro degradation of bone graft substitutes. Biomaterials 1992;13:297.
[6] Whang K, Thomas CH, Healy KE, Nuber G. A novel method to fabricate bioabsorbable scaffolds. Polymer 1995;36:837.
[7] van de Witte P, Eselbrugge H, Dijkstra PJ, van den Berg JWA, Feijen J. Phase transitions during membrane formation of polylactides. I. A morphological study of membranes obtained from the system polylactide–chloroform–methanol. J Membrane Sci 1996;113:223.
[8] van de Witte P, Dijkstra PJ, van den Berg JWA, Feijen J. Metastable liquid–liquid and solid–liquid phase boundaries in polymer–solvent systems. J Polym Sci, Part B: Polym Phys 1997;35:763.
[9] van de Witte P, Boorsma A, Esselbrugge H, Dijkstra PJ, van den Berg JWA, Feijen J. Differential scanning calorimetry study of phase transitions in poly(lactide)–chloroform–methanol systems. Macromolecules 1996;29:212.
[10] van de Witte P, Dijkstra PJ, van den Berg JWA, Feijen J. Phase separation processes in polymer solutions in relation to membrane formation. J Membrane Sci 1996;117:1.
[11] van de Witte P, Esselbrugge H, Dijkstra PJ, van den Berg JWA, Feijen J. A morphological study of membranes obtained from the systems polylactide–dioxane–methanol, polylactide–dioxane–water, and polylactide–*N*-methyl pyrrolidone–water. J Polym Sci, Part B: Polym Phys 1996;34:2569.
[12] van de Witte P, Dijkstra PJ, van den Berg JWA, Feijen J. Phase behavior of polylactides in solvent–non solvent mixtures. J Polym Sci, Part B: Polym Phys 1996;34:2553.
[13] van de Witte P, van den Berg JWA, Feijen J, Reeve JL, Mchugh AJ. In situ analysis of solvent/non solvent exchange and phase separation processes during the membrane formation of polylactides. J Appl Polym Sci 1996;61:685.
[14] Nunes SP, Inoue T. Evidence for spinodal decomposition and nucleation and growth mechanisms during membrane formation. J Membrane Sci 1996;111:93.
[15] Karnovsky MJ. A formaldehyde–glutaraldehyde fixative of high osmolality for use in electron microscopy. J Cell Biol 1965;27:136.
[16] Mello MLS, Vidal BC. In: Blucher E, editor. Practices in cellular biology, 1980: 69 (in Portuguese).
[17] Grinnell F, Bennett MH. Fibroblast adhesion on collagen substrate in the presence and absence of plasma fibronectin. J Cell Sci 1981;48:19.
[18] Horst R. Calculation of phase diagrams not requiring the derivatives of the Gibbs energy demonstrated for a mixture of two homopolymers

with the corresponding copolymer. Macromol Theory Simul 1995;4:449.
[19] Horst R. Calculation of phase diagrams not requiring the derivatives of the Gibbs energy for multinary mixtures. Macromol Theory Simul 1996;5:789.
[20] Reuvers AJ, van den Berg JWA, Smolders CA. Formation of membranes by means of immersion precipitation. Part I. A model to describe mass transfer during immersion precipitation. J Membrane Sci 1987;34:45.
[21] Reuvers AJ, Smolders CA. Formation of membranes by means of immersion precipitation. Part II. The mechanism of formation of membranes prepared from the system cellulose acetate–acetone–water. J Membrane Sci 1987;34:67.
[22] Wijmans JG, Rutten HJJ, Smolders CA. Phase separation phenomena in solutions of poly(2,6-dimethyl-1,4-phenylene oxide) in mixtures of trichloroethylene, 1-octanol and methanol: relationship to membrane formation. J Polym Sci, Part B: Polym Phys 1985;23:1941.
[23] Cahn JW, Hilliard JE. Free energy of a non uniform system. I. Interfacial free energy. J Chem Phys 1958;28:258.
[24] Wang Z, Konno M, Saito S. Kinetics of phase separation in polymer blends. Calculations based on nonlinear theory. J Polym Sci, Part B: Polym Phys 1993;32:461.
[25] Langer JS, Bar-on M, Miller HD. New computational method in the theory of spinodal decomposition. Phys Rev 1975;A11:1417.
[26] Cook HE. Brownian motion in spinodal decomposition. Acta Metall 1970;18:297.
[27] Golombick T, Dajee D, Bezwoda WR. Extracellular matrix interactions. I. Production of extracellular matrix with attachment and growth sustaining functions by UWOUS ovarian cancer cells growing in protein free conditions. Rev Biol 1995;31:387.
[28] Santos AR Jr. Effects of fetal calf serum and dexamethasone in the invasion and differentiation of VERO cells cultured on collagen I gel. MSc Thesis, Campinas State University, 1996 (in Portuguese).